Journal of
Micromechanics and
Microengineering

PURPOSE-LED
PUBLISHING™

3D-Printing the Spinneret: A single-piece microfluidic platform for tunable hydrogel fiber fabrication

To cite this article before publication: Niloofar Ghasemzaie *et al* 2026 *J. Micromech. Microeng.* in press https://doi.org/10.1088/1361-6439/ae553d

Journal Name

Crossmark

RECEIVED
dd Month yyyy

REVISED
dd Month yyyy

ARTICLE TYPE

3D-Printing the Spinneret: A single-piece microfluidic platform for tunable hydrogel fiber fabrication

Niloofar Ghasemzaie[1,2,3], Dario Bogojevic[2,3] and Scott S. H. Tsai[1,2,3,4,*]

[1]Biomedical Engineering Graduate Program, Toronto Metropolitan University, Toronto, ON M5B 2K3, Canada
[2]Keenan Research Centre for Biomedical Science, St. Michael's Hospital, Unity Health Toronto, Toronto, ON M5B 1T8, Canada
[3]Institute for Biomedical Engineering, Science and Technology (iBEST), Toronto, ON M5B 1T8, Canada
[4]Department of Mechanical, Industrial, and Mechatronics Engineering, Toronto Metropolitan University, Toronto, ON M5B 2K3, Canada

*Author to whom any correspondence should be addressed.

E-mail: scott.tsai@torontomu.ca

Keywords: 3D-printing, Aqueous two-phase system, Hydrogel fibers, Core–shell and Janus structures, Biofabrication

Abstract

We describe a single-piece 3D-printed aqueous two-phase system (ATPS) spinneret that eliminates the glass capillaries, alignment steps, and bonding required in polydimethylsiloxane (PDMS)–glass devices, collapsing multi-step fabrication into one print. The printed geometry preserves the coaxial flow needed for forming hydrogel fibers, including Janus structures, maintaining full functionality while removing fabrication complexity.

1 Introduction

Fibrous hydrogel constructs are attractive building blocks in biofabrication. Their high surface-to-volume ratio and interconnected porosity support cell adhesion and mass transport while enabling hierarchical assembly of tissues[1]. Microfluidic spinning uniquely controls fiber diameter, internal composition, and interfacial architecture under gentle, cell-compatible conditions[2, 3, 4]. Within this landscape, aqueous two-phase systems (ATPS) are attractive because their ultralow interfacial tension stabilizes thread formation, suppresses droplet breakup, and preserves sensitive cargos in an all-aqueous milieu[5, 6, 7].

Microfluidic approaches have enabled hydrogel fibers with diverse morphologies, including solid, hollow, core–shell, grooved, and Janus architectures, each supporting distinct mass transport and cell–matrix interactions[2, 3, 4, 8, 9, 10]. Yet their broader use is held back by the complexity of fabricating the spinning devices themselves. Existing platforms typically rely on hybrid PDMS–glass assemblies, which require multi-step molding, plasma bonding, and the manual insertion and alignment of fragile glass capillaries[11, 12, 13]. These assembly steps introduce operator dependence, increase device-to-device variability, and restrict scalability. Our group's previous hybrid PDMS–glass capillary ATPSpin device addressed the clogging caused by the immediate gelation of alginate by introducing an ATPS spacer that delayed cross-linker transport, stabilizing water-in-water threads and allowing a single device to generate multiple fiber morphologies. However, the ATPSpin technique still relied on laborious construction—merging a glass capillary with a PDMS device—and fragile glass components[14].

Here, we introduce a single-piece 3D-printed ATPSpin that removes glass capillaries, alignment, and bonding entirely by integrating the full ATPS spinning geometry into one 3D-printed structure. Advances in low-cost, high-resolution resin printing now allow coaxial microfluidic architectures to be fabricated directly from CAD designs, offering an accessible and reproducible route to single-step device production[15, 16]. Using this printed spinneret, we demonstrate ATPS fiber formation and simple CAD-level modification for Janus architectures[9, 8, 10].

2 Experimental

2.1 Chemical preparation

An ATPS was prepared following our previous ATPSpin protocol[14]. Dextran (DEX; 8% w/w, M_n 500 kDa) and Polyethylene glycol (PEG; 11.8% w/w, M_n 35 kDa) were dissolved in deionized water, mixed at 60 °C and then allowed to phase-separate overnight. The PEG-rich and DEX-rich phases were collected. For fiber spinning, alginate (1.5% w/v) was dissolved in the PEG-rich phase (Alg–PEG), and calcium chloride (3% w/v) was dissolved in PEG (Ca^{2+}–PEG), replacing the Ba^{2+} system used previously[14] due to Ca^{2+} biocompatibility[17]. Gellan gum (0.5% w/v) was added to the PEG-rich phase for Janus fibers. For fluorescence imaging, yellow-green beads (1.0 µm, Sigma L4655) were added to Alg–PEG and red beads (0.5 µm, Sigma) to the gellan gum solution.

2.2 Microfluidic Device Design and Fabrication

Devices were modeled in SolidWorks and fabricated using a ProFluidics 285D DLP microfluidic-specific 3D printer (CADworks3D, Canada) with Clear Microfluidic Resin (CADworks3D) at 30 μm layer resolution. Post-processing began with removal of the printed device from the build plate using a utility knife. Devices were submerged in IPA for ∼30 s, dried with an air gun, and flushed internally by connecting a syringe with tubing to each port and purging with IPA followed by compressed dry air. The devices were then UV-post-cured for 60 seconds using a CADworks curing zone instrument to complete polymer crosslinking. The complete post-processing workflow takes approximately 15 min; the print itself takes ∼2.5 hr. The ProFluidics 285D enables enclosed rectangular channels down to 80 μm (XY) × 250 μm (Z). Through iterative testing, the smallest reliably printable orifice was 150 μm × 150 μm (length 0.45 mm). Other channel cross-sections were 250 μm × 250 μm (post-orifice collection channel, length 3.2 mm), 400 μm × 400 μm (pre-outlet collection channel, length 16.7 mm), and 400 μm × 600 μm (supply channels, length >60 mm). The printed modules were then ready for microfluidic experiments. CAD design files (STL format) for both device variants are provided as supplementary material to facilitate reproduction (Files S1–S2).

2.3 Microfluidic Setup and Fiber Production

Flow injection into the printed ATPSpin device was achieved using PEEK tubing (OD = 1/16 in., ID = 0.020 in.; IDEX Health & Science, Oak Harbor, WA, USA). Flow rates were controlled by a pressure-driven system (Flow EZ, Fluigent, Paris, France) operated via the Microfluidic Automation Tool software[14]. For solid fibers, the four inlets were loaded with Alg–PEG (inlets 1 and 2), the DEX-rich phase (inlet 3), and Ca^{2+}–PEG (inlet 4). For hollow and droplet-filled fiber morphologies, the inlet configuration was modified by supplying the DEX-rich phase at the first inlet in place of Alg–PEG, while the other inlets remained unchanged. Core–shell architectures were obtained by adding 40% (v/v) poly(ethylene glycol) diacrylate (PEGDA, M_n 700 Da; Sigma-Aldrich) and 10% (v/v) lithium phenyl-2,4,6-trimethylbenzoylphosphinate (LAP) photoinitiator to the DEX-rich phase, using the same inlet configuration as for hollow fibers. Upon collection at the outlet, fibers were immediately exposed to 365 nm UV light from a curing lamp (Silkline Professional, model 22HUVLAMPNC; 12 mW cm^{-2} irradiance at 5 cm), for 5 s to polymerize the PEGDA core within the alginate shell. Janus architectures were generated by modifying only the first inlet of the coaxial configuration into a Y-shaped junction, allowing two aqueous streams to converge before entering the coaxial nozzle. From the left branch, Alg–PEG was introduced, while the right branch delivered gellan gum–PEG. The merged streams flowed side by side into the coaxial geometry and were subsequently cross-linked by Ca^{2+}–PEG, yielding stable Janus fibers. Collected fibers were subsequently washed and prepared for analysis.

2.4 Fiber Imaging

Bright-field images and videos were recorded with a high-speed camera (Miro M110, Vision Research, Wayne, NJ) mounted on an inverted microscope (Axio Observer A1, Carl Zeiss, Oberkochen, Germany). Fluorescent images of labeled fibers were acquired using blue and red channels of ZOE fluorescent cell imager (Bio-Rad). For SEM imaging, fibers were washed in deionized water, dehydrated through graded ethanol (50%, 70%, 100%; 20 min each), and dried via critical point drying. Imaging protocols were adapted from our earlier workflow[14].

3 Results and discussion

The single-piece 3D-printing approach removes the labor-intensive fabrication steps that limited the earlier platform[14]. As shown in Figure 1a, the PDMS–glass devices required multi-step molding, plasma bonding, manual alignment, and sealing of fragile glass capillaries, a process that

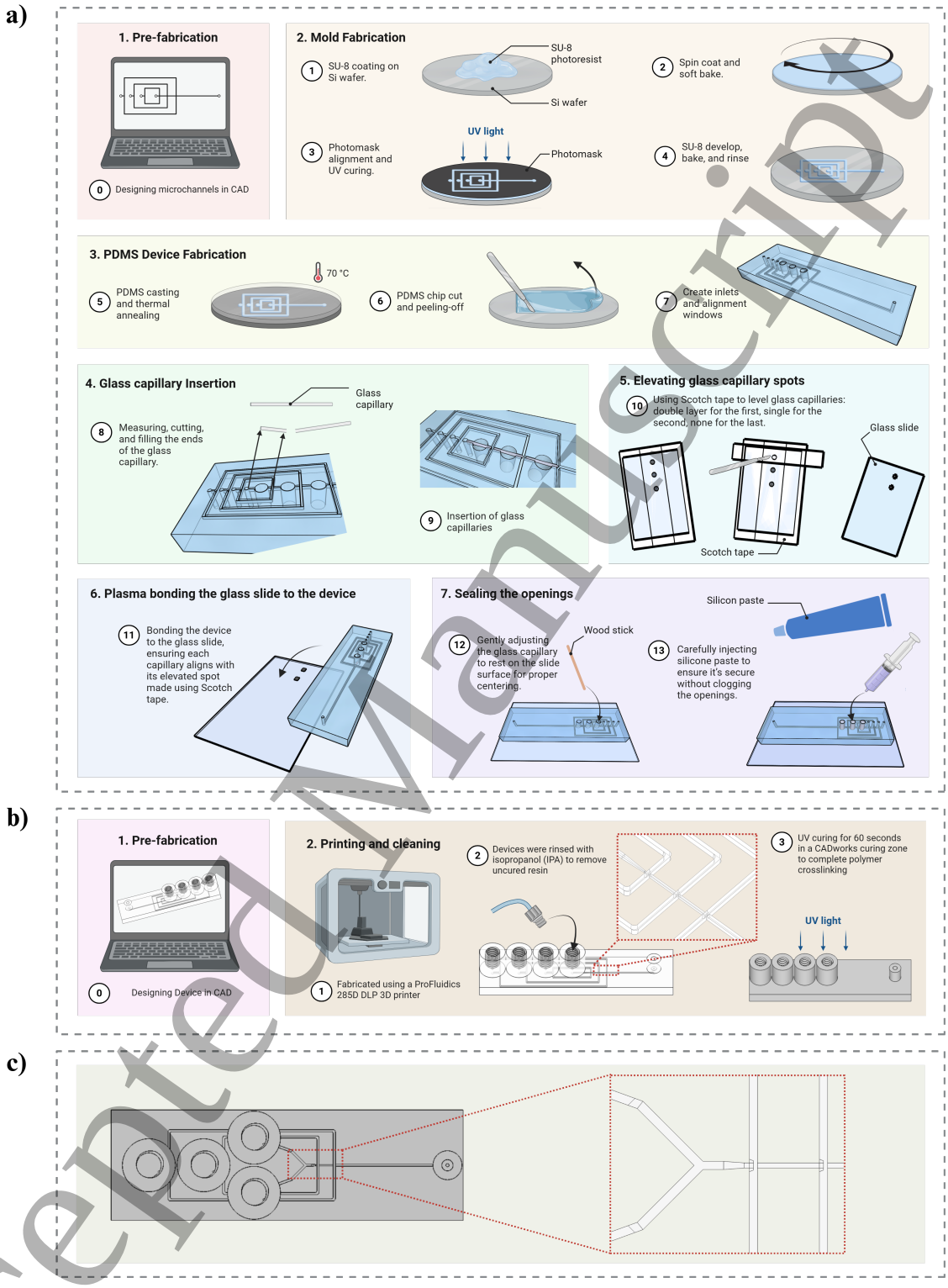

Figure 1. Evolution of the ATPSpin platform toward a fully 3D-printed device. (a) Workflow of the previous hybrid PDMS–glass capillary ATPSpin, requiring multi-step soft-lithographic fabrication and manual insertion and sealing of fragile glass capillaries. (b) The new ATPSpin condenses the entire assembly into a single stereolithography-printed component with integrated threaded inlets for direct pressure-driven operation. (c) Design flexibility enabled by additive manufacturing: a Y-shaped inlet can be incorporated into the same printed geometry to support Janus fiber formation.

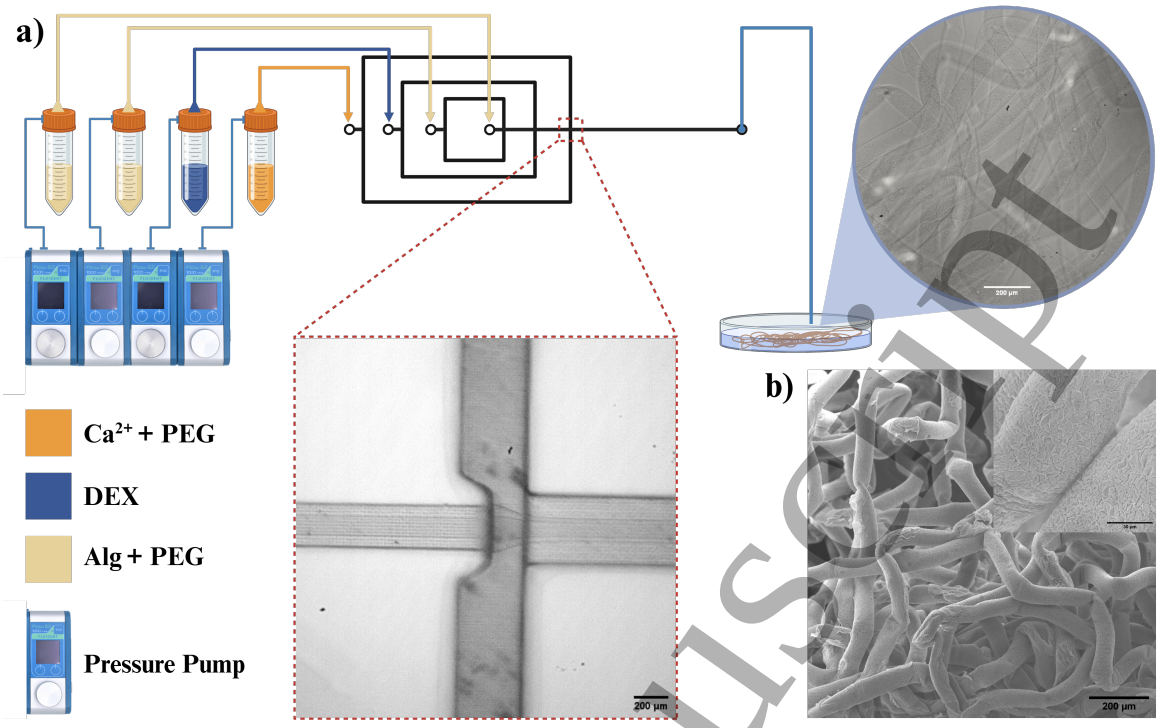

Figure 2. Fabrication of solid hydrogel fibers using the fully printed ATPSpin device. (a) Pressure-driven injection of Alg–PEG, DEX spacer, and Ca^{2+}–PEG into the printed coaxial nozzle forms a stable ATPS thread, shown in the magnified micrograph at the junction. The bright-field image illustrates the continuous solid fiber collected at the outlet (scale bars: 200 µm). (b) SEM images of the collected fibers confirming continuous solid morphology and uniform surface texture (scale bars: 200 µm and 50 µm).

demanded operator skill and resulted in high device rejection rates[18]. In contrast, DLP 3D-printing integrates all microfluidic features in a single step, including the coaxial flow geometry and the nozzles at the junction regions (Figure 1b). This direct realization of complex 3D channel architectures is a key advantage of additive manufacturing over planar soft lithography[18]. Incorporating fully 3D coaxial nozzles into PDMS devices would be extremely difficult, if not impossible. The coaxial configuration is crucial for centering the inner stream, maintaining a stable sheath, and preventing wall contact or clogging during fiber spinning[2]. The printed design preserves this coaxial flow-focusing principle and also enables modular features, such as Y-shaped inlet junctions for Janus fibers, without any assembly (Figure 1c). This flexibility reflects a broader shift toward 3D-printed microfluidics as a robust alternative to PDMS or capillary-based devices for advanced fiber-spinning applications[2]. Building on this integrated fabrication, the printed spinneret incorporates threaded inlet ports that form secure, leak-free seals with standard fittings and tubing. These screw-type connectors remove the frequent leakage, capillary slippage, and flow destabilization observed in the PDMS–glass device, particularly under elevated pressures or sudden pressure spikes from clogging. Press-fit inlets in the earlier setup occasionally produced hazardous spray-outs during stress events, whereas 3D-printed connectors withstand internal pressures of hundreds of kPa without leaking[18]. Connector compatibility was confirmed by repeated attachment and detachment of IDEX PEEK fittings without leakage or thread wear after standard post-processing (see Figures S1–S2). The rigid photopolymer construction further improves operational reliability by allowing the microchannels to be flushed at high pressure, which we routinely used to remove residual alginate or hydrogel debris. PDMS devices, by contrast, readily foul and irreversibly clog when exposed to protein- or hydrogel-based solutions; alginate gels rapidly on PDMS's hydrophobic walls and can permanently block channels[19]. In the printed device, such residues can be cleared by simple flushing, consistent with reports that 3D-printed microfluidics tolerate chemical or ultrasonic cleaning without damage[20].

Under pressure-driven flow, the 3D-printed device produced continuous Alg–PEG hydrogel fibers cross-linked on-chip by a calcium stream. Coaxial focusing at the nozzle yielded a stable three-phase flow configuration similar to that in our prior PDMS–capillary setup, indicating that the printed geometry retains the flow dynamics needed for continuous solid fiber spinning. We observed smooth, uninterrupted fibers collected at the outlet (Figure 2b). Scanning electron microscopy (SEM) confirmed these fibers had approximately uniform cylindrical geometry with no

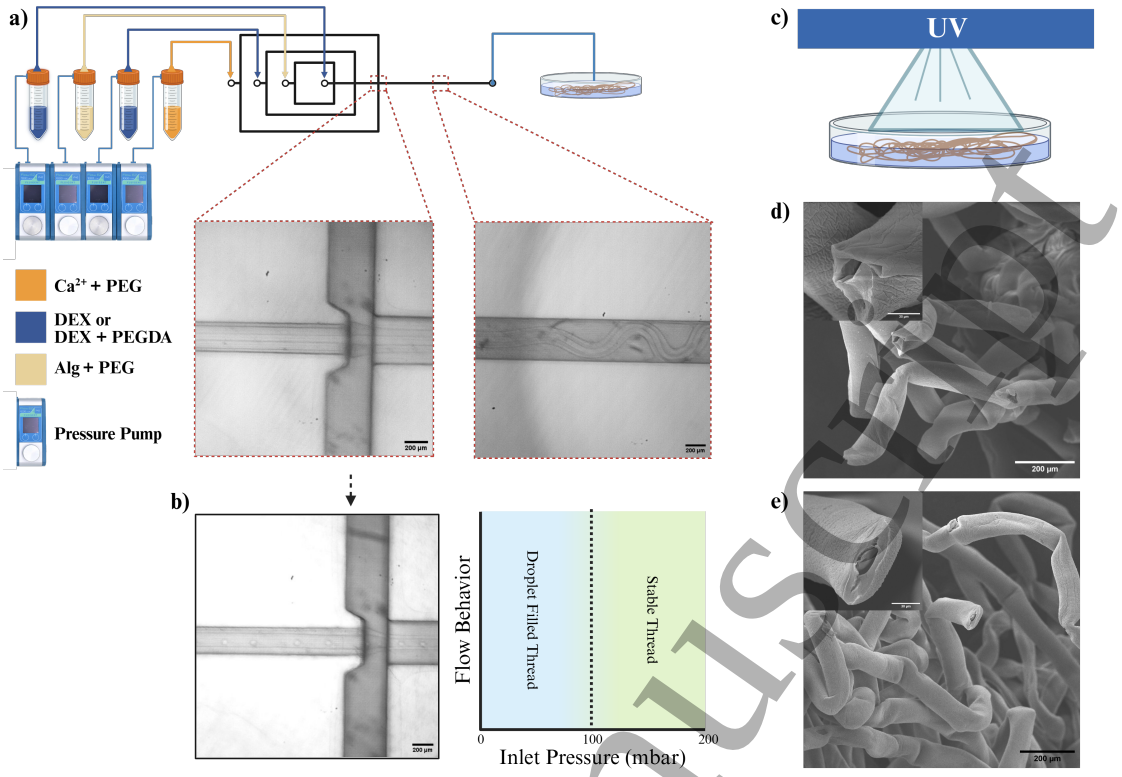

Figure 3. Pressure-controlled fabrication of hollow, core–shell, and droplet-filled hydrogel fibers. (a) Pressure-driven delivery of core, shell, spacer, and cross-linker solutions produces four-phase coaxial flow within the printed nozzle. The magnified junction micrograph shows the four-phase ATPS coaxial flow, whereas the downstream image shows the gelled thread taking on its characteristic wavy shape. (b) Droplet breakup of the core is visible in the bright-field image and corresponds to the pressure–behavior plot indicating a droplet regime below 100 mbar. (c) UV curing step used to solidify PEGDA-containing cores for core–shell architectures. (d) SEM images of hollow fibers showing uniform shell walls and clear lumens (main image scale bars = 200 µm and inset scale bars = 30 µm). (e) SEM images of core–shell fibers with solidified PEGDA cores encapsulated within alginate shells (main image scale bars = 200 µm and inset scale bars = 30 µm).

surface defects, demonstrating that the resin-based channels can reproducibly generate solid hydrogel fibers comparable in quality to those from traditional PDMS devices[2].

By switching the core inlet in the solid-fiber configuration from PEG–Alg to a blank DEX-rich phase, the device produced either hollow fibers or droplet-filled fibers depending on the inlet pressures. When the DEX phase maintained a stable continuous stream, the alginate sheath solidified around it and yielded hollow fibers with a well-defined lumen. At lower core pressures, however, the DEX stream could not remain continuous. Below roughly 100 mbar, interfacial tension exceeded viscous drag and caused the core to pinch off into discrete droplets inside the alginate sheath[21]. In ATPS systems like ours, the ultralow interfacial tension, on the order of 10^{-3} Nm^{-1}, enables this dripping behavior at relatively low pressure. In this higher-pressure regime, introducing 40% w/w PEGDA into the core and photopolymerizing it on collection produced core–shell fibers with a solidified inner core (Figure 3c). SEM imaging confirmed a homogeneous polymerized core within a uniform alginate shell (Figure 3e). These morphologies match those reported in earlier coaxial microfluidic fiber platforms, showing that the printed device preserves and extends their capabilities. Fiber diameter in the 3D-printed ATPSpin system remained pressure-dependent and tunable across all morphologies demonstrated, consistent with our earlier ATPSpin observations[14].

To showcase the versatility of our 3D-printed device, we fabricated Janus hydrogel fibers by incorporating a Y-junction at the core inlet. This modification allowed two distinct aqueous streams, in our case, an alginate solution and a gellan gum solution (each dissolved in PEG), to merge as parallel laminar flows before entering the coaxial nozzle. The twin streams were then focused concentrically by the surrounding DEX phase and cross-linked by the calcium sheath, yielding a continuous fiber with two compositionally distinct halves. Fluorescence microscopy of Janus fibers (Figure 4c) confirmed that the two polymer solutions remained separated. SEM analysis revealed each half's unique morphology (Figure 4d), reflecting the inherent material

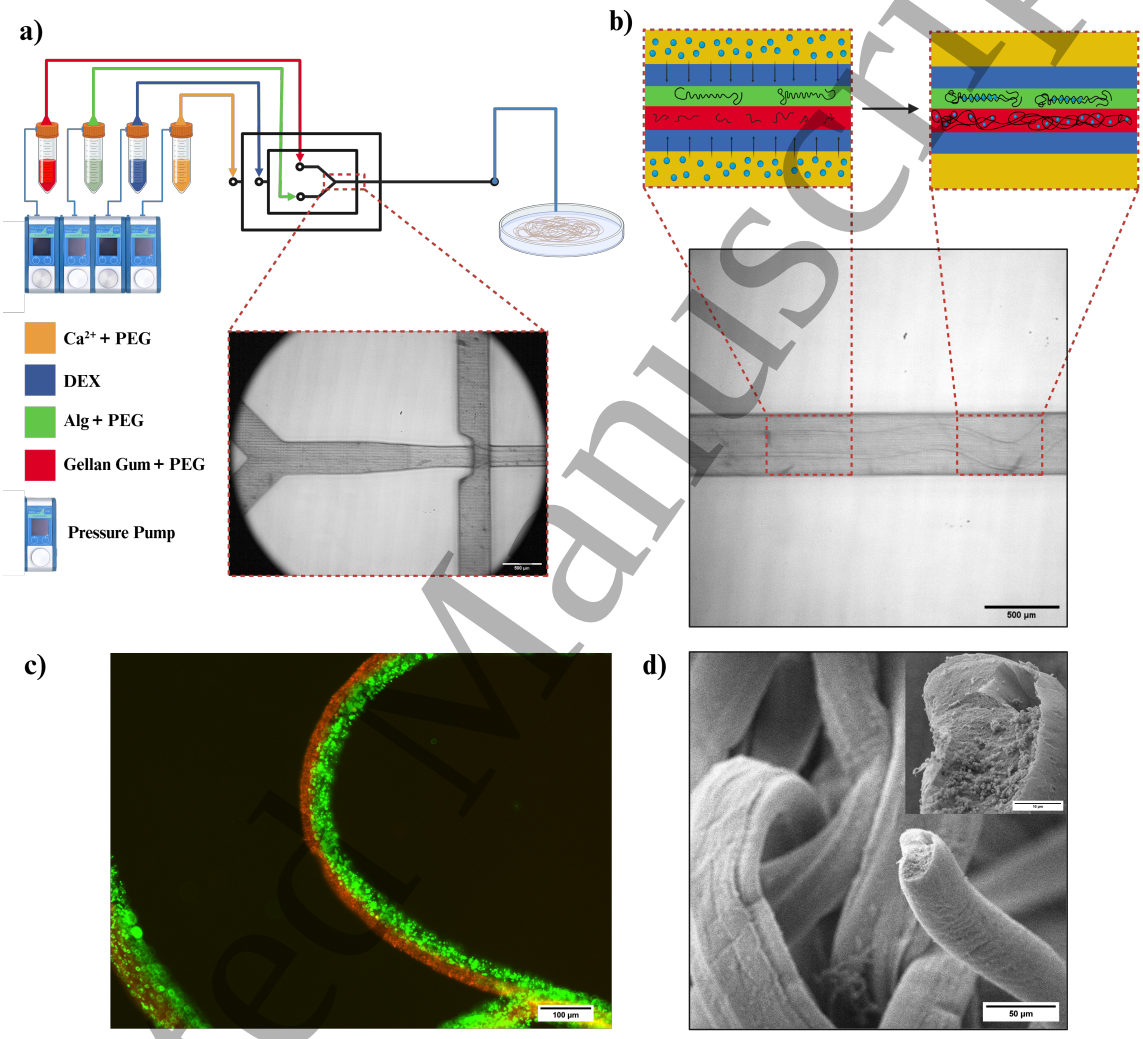

Figure 4. Janus hydrogel fiber formation using the Y-shaped ATPSpin device. (a) Pressure-driven co-flow of Gellan Gum–PEG (red) and Alg–PEG (green) at the Y-inlet, with DEX as the spacer and Ca^{2+}–PEG as the cross-linker. The nozzle micrograph shows side-by-side polymer streams focused by the DEX sheath (scale bar = 500 µm). (b) Schematic of Ca^{2+} diffusion through the DEX layer, with the downstream wavy pattern indicating progressive gelation (scale bar = 500 µm). (c) Fluorescence images of collected Janus fibers showing distinct Alg-rich (green) and Gellan Gum–rich (red) domains (scale bar = 100 µm). (d) SEM images confirming the two-region Janus morphology (main image scale bars = 50 µm and inset image scale bars = 10 µm).

differences (e.g. gellan gum vs alginate). The successful extrusion of continuous Janus fibers demonstrates that the printed platform can handle complex multi-stream flows and create hybrid structures. The formation of Janus microfibers using parallel co-flow in a microfluidic device is consistent with previous reports in the literature. For example, Jung *et al.* achieved Janus polyurethane microfibers by leveraging laminar multi-stream flow in a microfluidic chip[22]. In those fibers, each side had distinct properties (one porous, one non-porous), illustrating the same principle of maintaining separate phases within one filament[22].

4 Conclusion

The 3D-printed ATPSpin platform highlights how stereolithographic 3D-printing can simplify and improve aqueous two-phase microfluidic fiber fabrication. Integrating all geometries into a single printed component eliminates the need for glass capillaries and PDMS bonding while reproducing solid, hollow, core–shell, and Janus fiber morphologies. The rigid printed material withstands high-pressure flushing, allowing easy removal of hydrogel residues and repeated reuse. Threaded inlets prevent leakage under elevated pressures, addressing common failure modes in PDMS–glass devices such as capillary misalignment and fluid seepage. Collectively, these advances establish 3D-printed microfluidic systems as robust, accessible, and reproducible platforms for fiber-based biofabrication.

Acknowledgments

The authors thank Morteza Jeyhani for his helpful advice and for suggesting the 3D-printing approach used for device fabrication.

Funding

This work was supported by the Natural Sciences and Engineering Research Council of Canada (NSERC) Discovery Grants program (RGPIN-2025-04857), and the Canadian Institutes of Health Research (CIHR) Project Grants program (202303PJT-496149-BE2ABAF-244211). Equipment funding was from the Canada Foundation for Innovation (CFI, projects 36687 and 36442), the Ontario Research Fund (ORF), NSERC Research Tools and Instruments program (RTI-2024-00511), and Toronto Metropolitan University.

Authors contribution

N.G. performed the experiments, analyzed the data, and wrote the manuscript. D.B. designed and fabricated the CAD models, optimized the 3D-printing process, provided technical input on device design, and contributed to manuscript writing and editing. S.S.H.T. supervised the project, guided experimental design and data interpretation, and edited the manuscript.

Conflicts of interest

No Conflict of Interest.

References

[1] Afshin Abrishamkar, Azadeh Nilghaz, Maryam Saadatmand, Mohammadreza Naeimirad, and Andrew J deMello. Microfluidic-assisted fiber production: Potentials, limitations, and prospects. *Biomicrofluidics*, 16(6):061504, December 2022.

[2] Rodrigo Dores, Mónica S N Oliveira, and Luis M Bimbo. Microfluidic manufacture of composite fibers for biomedical applications. *Adv. Mater. Technol.*, September 2024.

[3] Jiahui Guo, Shuangshuang Miao, Lingyu Sun, Yuanjin Zhao, and Xiaosong Gu. Bioinspired micro-structured fibers for biomedical applications. *Bioact. Mater.*, 53:218–239, November 2025.

[4] Lang Nan, Huidan Zhang, David A Weitz, and Ho Cheung Shum. Development and future of droplet microfluidics. *Lab Chip*, 24(5):1135–1153, February 2024.

[5] Ehsan Atefi, J Adin Mann, Jr, and Hossein Tavana. Ultralow interfacial tensions of aqueous two-phase systems measured using drop shape. *Langmuir*, 30(32):9691–9699, August 2014.

[6] Andrea Fergola, Alberto Ballesio, Francesca Frascella, Lucia Napione, Matteo Cocuzza, and Simone Luigi Marasso. Droplet generation and manipulation in microfluidics: A comprehensive overview of passive and active strategies. *Biosensors (Basel)*, 15(6):345, May 2025.

[7] Yonggang Liu, Reinhard Lipowsky, and Rumiana Dimova. Concentration dependence of the interfacial tension for aqueous two-phase polymer solutions of dextran and polyethylene glycol. *Langmuir*, 28(8):3831–3839, February 2012.

[8] Chenguang Ouyang, Tian Tu, Haojie Yu, Li Wang, Zhipeng Ni, Jian Yang, Yanzhao Dong, Xiaodi Zou, Weijie Zhou, Jinyi Liu, Dingning Chen, Yu Wang, Xudong Wu, Hong Yi, Xunchun Yuan, Zhenfeng Liu, and Hui Lu. One-step formed janus hydrogel with time-space regulating properties for suture-free and high-quality tendon healing. *Adv. Sci. (Weinh.)*, 12(13):e2411400, April 2025.

[9] Yingxue Jiang, Chenhui Zhu, Xiaoxuan Ma, and Daidi Fan. Janus hydrogels: merging boundaries in tissue engineering for enhanced biomaterials and regenerative therapies. *Biomater. Sci.*, 12(10):2504–2520, May 2024.

[10] Mingfei Pan, Tao Shui, Ziqian Zhao, Li Xiang, Bin Yan, Ning Gu, and Hongbo Zeng. Engineered janus hydrogels: biomimetic surface engineering and biomedical applications. *Natl. Sci. Rev.*, 11(10):nwae316, October 2024.

[11] Lawrence W Honaker, Shameek Vats, Manos Anyfantakis, and Jan P F Lagerwall. Elastic sheath–liquid crystal core fibres achieved by microfluidic wet spinning. *J. Mater. Chem. C Mater. Opt. Electron. Devices*, 7(37):11588–11596, 2019.

[12] Kazutoshi Iijima, Shun Ohyama, Kazuya Yuyama, Atsushi Shono, and Mineo Hashizume. Selective fabrication of hollow and solid polysaccharide composite fibers using a microfluidic device by controlling polyion complex formation. *Polym. J.*, 50(12):1187–1198, December 2018.

[13] Bhargav Krishna Pullagura and Venkat Gundabala. Microfluidics-based on-demand generation of nonwoven and single polymer microfibers. *Langmuir*, 36(5):1227–1234, February 2020.

[14] Niloofar Ghasemzaie, Morteza Jeyhani, Kushal Joshi, Warren L Lee, and Scott S H Tsai. ATPSpin: A single microfluidic platform that produces diversified ATPS-alginate microfibers. *ACS Biomater. Sci. Eng.*, 10(6):3896–3908, June 2024.

[15] Cristiane Kalinke and Rodrigo A A Muñoz. 3D-printed microdevices: From design to applications. *Micromachines (Basel)*, 15(6):791, June 2024.

[16] Houda Shafique, Vahid Karamzadeh, Geunyong Kim, Molly L Shen, Yonatan Morocz, Ahmad Sohrabi-Kashani, and David Juncker. High-resolution low-cost LCD 3D printing for microfluidics and organ-on-a-chip devices. *Lab Chip*, 24(10):2774–2790, May 2024.

[17] Yrr A Mørch, Ivan Donati, Berit L Strand, and Gudmund Skjåk-Braek. Effect of Ca2+, Ba2+, and Sr2+ on alginate microbeads. *Biomacromolecules*, 7(5):1471–1480, May 2006.

[18] Sidra Waheed, Joan M Cabot, Niall P Macdonald, Trevor Lewis, Rosanne M Guijt, Brett Paull, and Michael C Breadmore. 3D printed microfluidic devices: enablers and barriers. *Lab Chip*, 16(11):1993–2013, 2016.

[19] Kevin Enck, Shiny Priya Rajan, Julio Aleman, Simone Castagno, Emily Long, Fatma Khalil, Adam R Hall, and Emmanuel C Opara. Design of an adhesive film-based microfluidic device for alginate hydrogel-based cell encapsulation. *Ann. Biomed. Eng.*, 48(3):1103–1111, March 2020.

[20] Chengpeng Chen, Benjamin T Mehl, Akash S Munshi, Alexandra D Townsend, Dana M Spence, and R Scott Martin. 3D-printed microfluidic devices: Fabrication, advantages and limitations-a mini review. *Anal. Methods*, 8(31):6005–6012, August 2016.

[21] Andrew S Utada, Alberto Fernandez-Nieves, Howard A Stone, and David A Weitz. Dripping to jetting transitions in coflowing liquid streams. *Phys. Rev. Lett.*, 99(9):094502, August 2007.

[22] Jae-Hoon Jung, Chang-Hyung Choi, Seok Chung, Young-Min Chung, and Chang-Soo Lee. Microfluidic synthesis of a cell adhesive janus polyurethane microfiber. *Lab Chip*, 9(17):2596–2602, September 2009.